

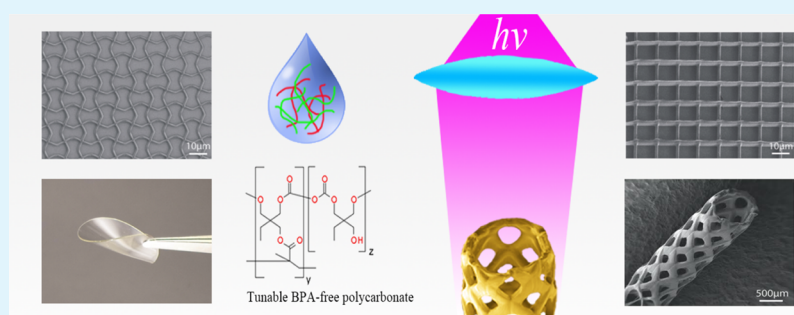
# Three-Dimensional Printing of Bisphenol A-Free Polycarbonates

Wei Zhu,<sup>†</sup> Sang-Hyun Pyo,<sup>\*,‡</sup> Pengrui Wang,<sup>†</sup> Shangting You,<sup>†</sup> Claire Yu,<sup>†</sup> Jeffrey Alido,<sup>†</sup> Justin Liu,<sup>†</sup> Yew Leong,<sup>†</sup> and Shaochen Chen<sup>\*,†</sup>

<sup>†</sup>Department of NanoEngineering, University of California, San Diego, La Jolla, California 92093, United States

<sup>‡</sup>Division of Biotechnology, Center for Chemistry and Chemical Engineering, Lund University, Box 124, SE-221 00 Lund, Sweden

## Supporting Information



**ABSTRACT:** Polycarbonates are widely used in food packages, drink bottles, and various healthcare products such as dental sealants and tooth coatings. However, bisphenol A (BPA) and phosgene used in the production of commercial polycarbonates pose major concerns to public health safety. Here, we report a green pathway to prepare BPA-free polycarbonates (BFPs) by thermal ring-opening polymerization and photopolymerization. Polycarbonates prepared from two cyclic carbonates in different mole ratios demonstrated tunable mechanical stiffness, excellent thermal stability, and high optical transparency. Three-dimensional (3D) printing of the new BFPs was demonstrated using a two-photon laser direct writing system and a rapid 3D optical projection printer to produce structures possessing complex high-resolution geometries. Seeded C3H10T1/2 cells also showed over 95% viability with potential applications in biological studies. By combining biocompatible BFPs with 3D printing, novel safe and high-performance biomedical devices and healthcare products could be developed with broad long-term benefits to society.

**KEYWORDS:** bisphenol A-free polycarbonate, BPA, 3D printing, photopolymerization, two-photon laser direct writing, continuous 3D projection printing, biomedical devices, healthcare products

## 1. INTRODUCTION

Eliminating the use of hazardous substances remains a global challenge to protect the human health, wildlife, and natural environment. Over the past decade, increasing efforts have been made to develop biocompatible and nontoxic materials for the manufacturing of biomedical devices, food, and healthcare products.<sup>1,2</sup> Naturally derived polymers such as polysaccharides (alginate, starch, and hyaluronic acid) and proteins (collagen and silk fibroin) have been frequently used in biomedical devices and other biological applications because of their excellent bioresorbability, low toxicity, and low manufacture and disposal costs.<sup>3</sup> However, the physical and mechanical properties of natural polymers do not always match the desired properties of biological tissues and biomedical devices. There are also limited methods to process these natural polymers into scaffolds or devices with complex structural designs. To address these challenges, novel synthetic biomaterials are being developed to enable higher control over material properties and meet the demands for medical research and clinical uses.<sup>4–6</sup>

Polycarbonates have been used for a wide range of applications, including food packages, drink bottles, water supply pipes, and a variety of healthcare products such as dental sealants and tooth coatings.<sup>7–10</sup> However, conventional polycarbonates are synthesized by either the polymerization of 2,2-bis(4-hydroxyphenyl)propane (bisphenol A, BPA) with highly toxic phosgene or diphenyl carbonate derived from the reaction of phenol and phosgene.<sup>11</sup> BPA is a known estrogen analogue which can disrupt the human endocrine system.<sup>12</sup> In consequence, a growing number of recent human studies have demonstrated the association between BPA exposure and adverse health issues including altered sex hormone concentrations, reduced male sexual function, premature delivery, blunted immune function, cardiovascular diseases, diabetes, obesity, and altered liver function.<sup>12–14</sup> In particular, early BPA exposure was found to be strongly correlated with behavioral changes and disrupted neurodevelopment in children.<sup>12,15,16</sup>

**Received:** December 1, 2017

**Accepted:** January 18, 2018

**Published:** January 18, 2018

With the prevalence of BPA-containing consumer products in which the majority are made using conventional polycarbonates, humans are exposed to BPA through their diet and dermal contact. This is supported in recent studies having shown that BPA is detected in the urine of approximately 95% of the adults and children.<sup>15,17,18</sup> Currently, BPA has been declared as a harmful substance in many countries including the United States, Canada, the European Union, and Norway.<sup>19</sup> In 2012, the U.S. Food and Drug Administration (FDA) banned the use of BPA in baby bottles and sippy cups, which prompted increased public attention and pressure to develop BPA-free polycarbonates (BFPs) for consumer products and medical devices.

Over the past decade, aliphatic polycarbonates have emerged as a new class of biocompatible BFPs because of the growing awareness of the risks of BPA exposure from aromatic polycarbonates.<sup>10</sup> Aliphatic polycarbonates can be obtained via ring-opening polymerization (ROP) of their respective cyclic monomers involving mainly five-membered cyclic carbonates (SCCs) and six-membered cyclic carbonates (6CCs).<sup>20</sup> Because of their intrinsic thermodynamic properties, the ROP of SCCs involves partial decarboxylation and thus introduces undesired ether linkages to the resulting polycarbonates. In contrast, 6CCs are thermodynamically more favorable monomers for producing polycarbonates without decarboxylation, and the functional groups on the 6CCs can be modified for additional properties.<sup>20</sup> However, the industrial production of commercial aliphatic polycarbonates involves toxic phosgene in the reaction, thus raising another safety concern.<sup>20</sup> As a result, there remains a need for a robust and green synthesis route of aliphatic polycarbonates.

Current manufacturing techniques for polycarbonate products are still limited to traditional machining, using mill and lathe, molding, and fused deposition modeling (FDM). A more versatile and efficient method to build polycarbonate devices has yet to be developed, especially for biomedical and healthcare applications. Recently, with the proven flexibility, FDM or selective laser sintering (SLS) three-dimensional (3D) printing techniques have been explored to manufacture devices with conventional BPA-containing polycarbonates. Notably, both FDM and SLS print in a serial raster scanning fashion (line by line), which provides a limited printing speed and potentially compromised the mechanical integrity because of the interfaces between the lines. Here, we report a novel reaction pathway to synthesize BFPs from functional 6CCs using a two-step polymerization method involving thermal ROP and light-induced free-radical polymerization (ROP-FRP). This unique synthesis route including photopolymerization enables us to use a microscale continuous optical projection printer ( $\mu$ COP) and a femtosecond laser direct writing (LDW) system to build complex 3D structures with nano- and microscale resolutions. Moreover, by altering the mole ratios of the reactants and the degree of cross-linking in the photopolymerization step, we can control the physical properties of the resulting polycarbonates. The mechanical, thermal, and optical properties of the BFP structures prepared from four different formulations were evaluated to demonstrate the material tunability. Finally, an *in vitro* study was conducted by seeding C3H10T1/2 cells in a monolayer onto BFP films to assess the biocompatibility.

## 2. EXPERIMENTAL METHODS

**2.1. Materials.** Methacrylated trimethylolpropane cyclic carbonate (TMPMAC, 97% technical grade) and nonfunctionalized trimethylolpropane cyclic carbonate (TMPC, 98% technical grade) were kindly prepared and provided by Cycliger AB (Sweden) according to previous work.<sup>21–23</sup> Triethylamine (TEA) and 1-propanol were purchased from Sigma-Aldrich (USA). A versatile photoinitiator for the radical polymerization of an unsaturated monomer, Irgacure 819 (bis(2,4,6-trimethylbenzoyl)-phenylphosphineoxide), was a product of BASF (Germany). All chemicals were used without further treatment.

**2.2. Preparation of BFP Prepolymers Functionalized with Methacrylate.** BFP prepolymers were prepared from TMPMAC and TMPC at different mole ratios (4/0, 3/1, 2/2, and 1/3) by ROP. For instance, in the case of a 2/2 ratio reaction, 0.2 mmol (45.6 mg) of TMPMAC and 0.2 mmol (32.4 mg) of TMPC were placed in a 1.5 mL vial, followed by the addition of 1% TEA and 1% 1-propanol in a chemical hood. The mixture was heated in a heating block at 80 °C, and the melted reactant was vortexed for 10 s. The BFP prepolymer was prepared by further heating in the heating block for 5 min. The resulting reactant was analyzed by Fourier transform infrared (FT-IR) spectroscopy and was used for making the thin film and 3D printing.

**2.3. Preparation of BFP Films.** In the above resulting liquid phase of BFP prepolymer, 1% Irgacure 819 was added and mixed. The resulting solution was placed in a poly(dimethylsiloxane) (PDMS) compartment and covered with another PDMS compartment. The height between the two compartments was held constant by PDMS spacers with a thickness of 100  $\mu$ m. The BFP films were then prepared by UV polymerization using a portable UV lamp at 365 nm.

**2.4. Characterization of Polycarbonates by FT-IR, Mechanical Tester, UV-Vis Spectrometry, Differential Scanning Calorimetry, Thermogravimetric Analysis, and Scanning Electron Microscopy.** The reactions of ROP and photopolymerization were monitored based on the transformation of functional groups such as hydroxyl, carbonyl, and alkene by FT-IR. The spectra of samples were obtained in the region of 4000–500  $\text{cm}^{-1}$  using a Spectrum Two spectrometer (PerkinElmer). An air background spectrum was collected before the analysis of the sample and subtracted from each sample spectrum.

The Young's moduli of the BFP samples were measured using the CellScale UniVert mechanical tester (CellScale, Waterloo, Canada) via compression testing at a strain rate of  $6.7 \times 10^{-3} \text{ s}^{-1}$  ( $n = 3$  per BFP formulation). Young's modulus was calculated from the linear strain region (5–10%). The data are reported as mean  $\pm$  standard deviation. Optical transmissions of the thin BFP films were measured from 300 to 1000 nm using a UV-vis spectrophotometer (Infinite 200 PRO, Tecan, Männedorf, Schweiz). Differential scanning calorimetry (DSC) was carried out using DSC Q20 (TA Instrument) over a temperature range from 0 to 180 °C, increasing 10 °C/min under nitrogen. Thermogravimetric analysis (TGA) was performed using Pyris 1 TGA (PerkinElmer) from 20 to 200 °C, increasing 10 °C/min under nitrogen. High-resolution scanning electron microscopy (SEM) images were obtained using Zeiss Sigma 500. The surface of the structure was coated with iridium by an Emitech K575X sputter coater prior to imaging.

**2.5. Three-Dimensional Printing Using the Two-Photon LDW System.** The two-photon LDW system utilizes a Ti:sapphire near-infrared femtosecond laser (800 nm) as the light source and a 100 $\times$  oil immersion objective lens on the Nikon microscope to focus the laser beam for fabrication.<sup>24,25</sup> A set of optics were placed between the Nikon microscope and the laser head to expand and collimate the laser beam. The computer controlled the laser source and the 3D automated stage to print microstructures according to the 3D models. A charge-coupled device camera was used to monitor the 3D fabrication in real time. Irgacure 819 (1%) was added and mixed to the BFP prepolymer solution for the 3D printing process using the two-photon LDW system.

**2.6. Three-Dimensional Printing Using  $\mu$ COP.** The  $\mu$ COP system consists of a digital micromirror array device (DMD) chip (Texas Instrument, USA), a light source (405 nm), projection optics, a motorized stage, and a computer.<sup>26,27</sup> A motorized syringe pump

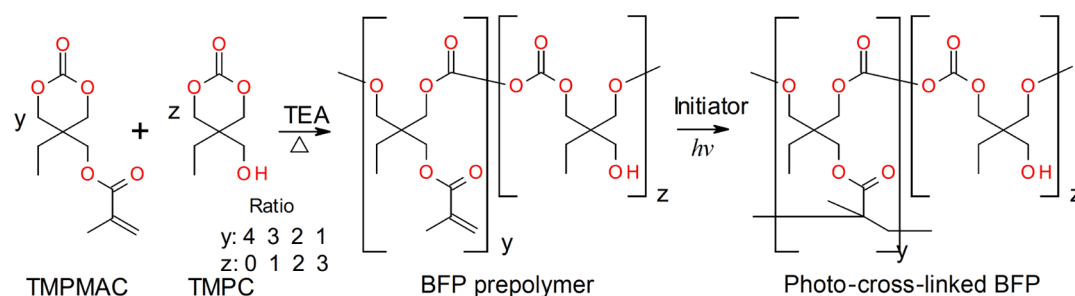


**Figure 1.** Synthesis pathway of the BFPs. BFPs are prepared from cyclic carbonates by a two-step process consisting of thermal ROP and photoinduced polymerization.

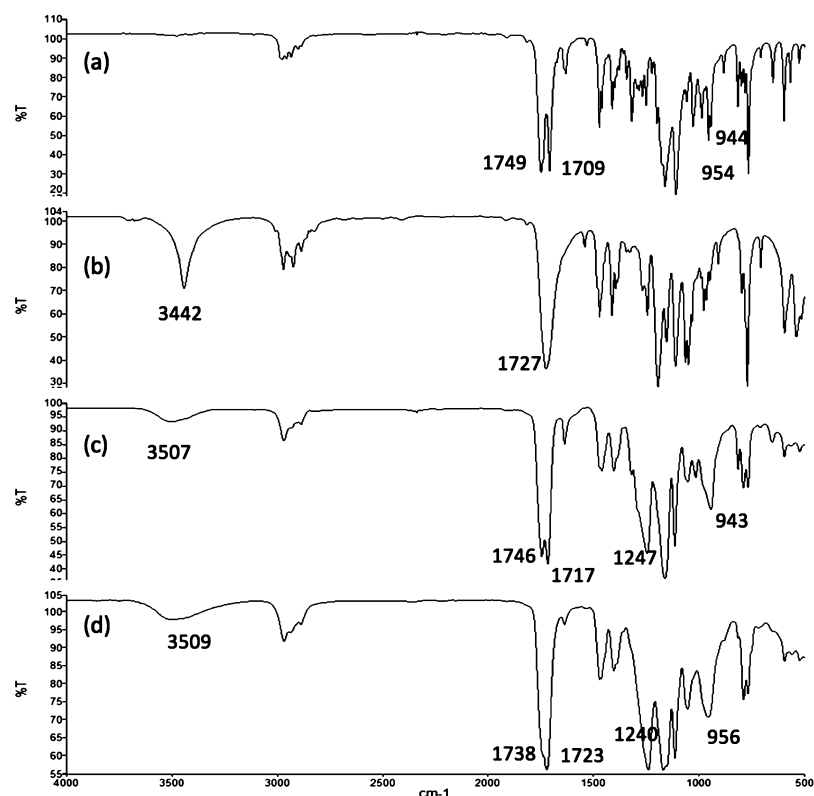


**Figure 2.** FT-IR spectrum for the representative preparation process of the BFPs. (a) TMPMAC, (b) TMPC, (c) polycarbonate prepolymer prepared from TMPMAC and TMPC at a ratio of 3:1 by thermal ROP, and (d) polycarbonate cross-linked on the methacrylate group from the polycarbonate prepolymer (c) by photopolymerization.

system can be used to add the prepolymer solution to the fabrication reservoir. The computer slices the 3D model into a series of digital masks and sends them to the DMD chip continuously. The DMD chip is composed of approximately 4 million micromirrors which can be controlled by each pixel on the digital masks individually. The optical patterns generated on the DMD (corresponding to the digital masks) project the light to the prepolymer solution loaded onto the stage. By simultaneously updating the digital masks and moving the stage, 3D objects are printed continuously. Irgacure 819 (1%) was added and mixed to the BFP prepolymer solution for the 3D printing process using the  $\mu$ COP system.

**2.7. Cell Viability Assay.** Before cell seeding, each BFP film was placed in a 24-well plate and equilibrated in 500  $\mu$ L of cell culture medium overnight at 37  $^{\circ}$ C with 5% CO<sub>2</sub>. The cell culture medium consisted of 10% fetal bovine serum (Gibco) and 1% penicillin–streptomycin (Gibco) in Dulbecco’s modified Eagle medium (Gibco). The next day, C3H10T1/2 cells were seeded on the BFP films at a density of 5000 cells per well. A cell viability assay (LIVE/DEAD viability/cytotoxicity kit, Invitrogen) was performed at 24, 48, and 96 h after the seeding. The samples ( $n = 3$  for each BFP formulation per

time point) were washed with Dulbecco’s phosphate-buffered saline (Gibco) once after removing the culture medium. Each sample was then stained with 2 mM calcein AM (live cell stain) and 4 mM ethidium homodimer-1 (dead cell stain) solution at room temperature for 30 min. After incubation, the samples were gently washed to remove the residual dye. Fluorescence images of the samples were taken immediately using a Leica DMI 6000B microscope (10 $\times$  objective, Leica Microsystems) for quantification. The live and dead cells were counted manually in a blinded experiment for each sample using ImageJ analysis. The data are reported as mean  $\pm$  standard deviation.

### 3. RESULTS AND DISCUSSION

**3.1. Synthesis of BFPs.** To prepare BFPs, we synthesized two types of 6CCs: TMPMAC and nonfunctionalized TMPC.<sup>21–23</sup> BFPs were then prepared from a mixture of these two cyclic carbonates in different ratios by the ROP–FRP process involving the ROP of the cyclic carbonates and photopolymerization of the methacrylate functional group

(Figure 1). The 6CCs were first thermally ring-opened to produce an intermediate polycarbonate prepolymer at 80 °C. TEA (1%) and 1-propanol (1%) were used as catalysts for the ROP. Organocatalysts, including amines (*N,N*-dimethylamino-pyridine, *N,N*-dimethylaniline, TEA, and pyridine), guanidine (1,5,7-triazabicyclo-[4.4.0]dec-5-ene), and phosphazene [2-*tert*-butylimino-2-diethylamino-1,3-dimethylperhydro-1,3,2-diazaphosphorine], have been widely used in the ROP of cyclic monomers.<sup>28</sup> These organocatalysts, used in the presence of alcohol (e.g., benzyl alcohol, 1-propanol, 1,3-propanediol, and glycerol; up to 20 equiv), in solution or in bulk, operate through an activated-monomer mechanism. Alcohol acts as both a coinitiator and a chain-transfer agent.

The intermediate polycarbonate prepolymer was then further photopolymerized by the methacrylate group to form the final polycarbonate structure. These reactions were accomplished by using only heat and a low-intensity light as a green process with mild conditions. In this study, four different mole ratios of the two reactant cyclic carbonates were chosen to investigate the effects on material properties: (1) 4:0, (2) 3:1, (3) 2:2, and (4) 1:3 mole ratios of TMPMAC and TMPC. The resulting BFPs are referred to as BFP-1, BFP-2, BFP-3, and BFP-4, respectively. After thermal ROP, the intermediate prepolymer was loaded onto the 3D optical printers to build 3D structures via the second photopolymerization step.

**3.2. FT-IR Spectroscopy of the Polymerization Process.** The transformation of the functional groups during the two-step reaction of thermal ROP and photopolymerization was monitored using FT-IR spectroscopy. A representative FT-IR spectrum from the synthesis process of BFP-2 (made from the 3:1 mole ratio of TMPMAC and TMPC) is shown in Figure 2. In the first ROP step to produce an intermediate polycarbonate prepolymer, the 1709 cm<sup>-1</sup> carbonyl group peak of TMPMAC (Figure 2a) and the 1727 cm<sup>-1</sup> carbonyl group peak of TMPC (Figure 2b) disappeared and merged as a new carbonyl peak at 1717 cm<sup>-1</sup> (Figure 2c). The 1749 cm<sup>-1</sup> peak of the carbonyl group next to the methacrylate group in TMPMAC (Figure 2a) was retained at 1746 cm<sup>-1</sup> (Figure 2c). A new broad peak at 1247 cm<sup>-1</sup> was attributed to the asymmetric stretching adsorption of the new C–O group formation by ROP (Figure 2c). The intermediate polycarbonate prepolymer remained as a liquid after the first step of ROP.

During the second step, where the intermediate polycarbonate prepolymer was further polymerized by free-radical polymerization, the 943 cm<sup>-1</sup> peak associated with the C–H bond in the monosubstituted alkene of methacrylate group (Figure 2c) disappeared because of the new C–C bond formation by photopolymerization (Figure 2d). The 1746 cm<sup>-1</sup> peak of the carbonyl group next to the methacrylate group in the intermediate copolycarbonate was shifted to 1738 cm<sup>-1</sup> and overlapped with the carbonyl peak of resulting polycarbonate at 1723 cm<sup>-1</sup> (Figure 2d). This process provides a novel, facile, and environmentally friendly approach for the synthesis of aliphatic polycarbonates without using hazardous raw materials or reaction conditions. Moreover, the combinational use of TMPMAC and nonfunctionalized TMPC can provide different degrees of cross-linking to produce BFPs with tunable physical properties.

**3.3. Mechanical, Thermal, and Optical Properties of BFPs.** The BFP films prepared from the two-step ROP–FRP process showed a high transparency with varied mechanical properties. To illustrate, flat and folded BFP-3 polycarbonate

films in Figure 3a,b demonstrate the optical transparency and flexibility of the final material. The Young's moduli of the BFPs

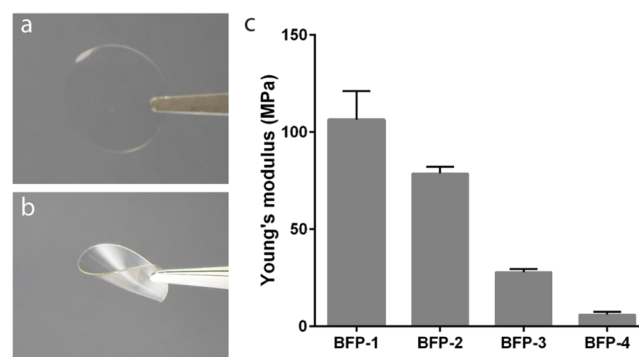


**Figure 3.** Mechanical properties of the BFPs. (a,b) Representative flat and folded films of BFPs prepared from TMPMAC and TMPC at a mole ratio of 2:2 (BFP-3). (c) Young's modulus (MPa) of BFPs prepared from TMPMAC and TMPC at mole ratios of 4:0 (BFP-1), 3:1 (BFP-2), 2:2 (BFP-3), and 1:3 (BFP-4).

with different compositions were measured by compression tests and are presented in Figure 3c. The mechanical measurement of BFP-1, BFP-2, BFP-3, and BFP-4 reveals a wide range of stiffness ranging from below 10 MPa to above 100 MPa. These mechanical properties can be further adjusted by the mole ratio of the two reactant carbonates, the photoinitiator concentration, the light exposure intensity, and time. As the mechanical properties of the matrix materials (e.g., stiffness) have been demonstrated to have major influences on the cell–matrix interactions and cell behaviors,<sup>29–33</sup> the tunability of the BFPs and the ROP–FRP process can be potentially employed to create customized scaffolds or devices for specific biological studies or medical applications.

Next, the thermal property of the new polycarbonates was evaluated by DSC, as shown in Figure 4a. The smooth energy flow during both heating and cooling processes indicated the lack of internal crystallinity in all four BFP formulations. Furthermore, the data from DSC also indicated that there was no thermal degradation of the new polycarbonate material from 0 to 180 °C and the chemical structure and morphology of the samples were maintained in repeated cycles. The glass-transition temperature ( $T_g$ ) was not observed from the DSC data potentially because of the cross-linked chemical structure of the material. TGA was performed to further investigate the thermal stability of the material from 20 to 200 °C (Figure S1). Similarly, TGA does not show thermal degradation of the material, and the morphologies of the samples were maintained over the measurement. From 20 to 200 °C, the material weight percentage changed from 100 to 98%, and the weight change started from the material being heated over 100 °C, which indicated that this insignificant weight change might be due to the evaporation of a small amount of residual water in the polymer material. The thermal stability indicates that these BFPs can be potentially used for applications involving high-temperature environments, such as autoclaving, which is commonly used to sterilize biomedical devices and surgical instruments for in vivo implantations or in vitro cell culture. Future analyses such as thermal expansion and thermal transition coefficient will be required to fully characterize the thermal properties.

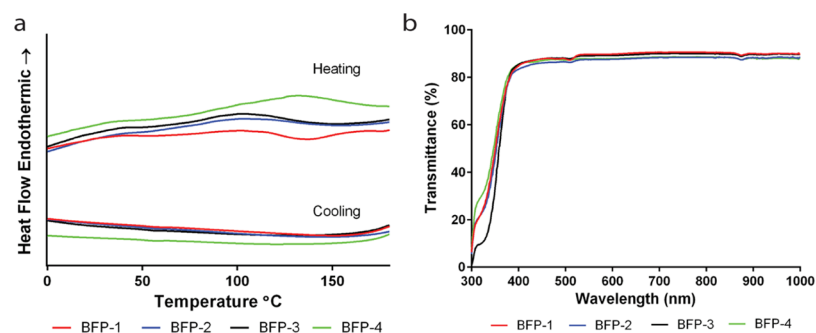


**Figure 4.** Thermal and optical properties of the BFPs. (a) Thermal properties of the BFPs measured by DSC. (b) Optical transmittances of the BFPs.

In addition to characterizing the mechanical and thermal properties, optical transparencies of the four BFP formulations were also measured by UV–vis spectrometry (Figure 4b). The transmittances of all four formulations were above 85% within the wavelength range of 400–1000 nm, which are comparable to that of the conventional BPA polycarbonates.<sup>34</sup> The high optical transparency of these BFPs also enables us to use them in our 3D printing platforms. The working wavelength of our femtosecond LDW platform is 800 nm, and the wavelength of the optical projection 3D printer is 405 nm. Furthermore, the high optical transparency makes these BFPs a promising material for use in a wide variety of biological applications where real-time high-resolution imaging is frequently used, ranging from organ-on-a-chip to microfluidic devices and customized cell culture vessels.

### 3.4. Two-Photon LDW with BPA-Free Polycarbonates.

To demonstrate the printability of the newly developed BFP materials, we adapted a two-photon LDW system<sup>24,25</sup> to three-dimensionally print the BFP structures with a submicron resolution (Figure 5). The intermediate polycarbonate prepolymer solution was loaded into the LDW system immediately after the thermal ROP step. The two-photon polymerization uses near-infrared femtosecond laser pulses (a wavelength of 800 nm) focused through a high-magnification (100 $\times$ ) objective lens to trigger the cross-linking of the photosensitive materials, during which two photons are absorbed simultaneously to generate free radicals. The stage loaded with the prepolymer solution moves in three dimensions, which enables the direct 3D writing of the polymer structure. The actual patterning can be programmed and controlled by computer-aided design software. Furthermore, the writing width can be tuned by the exposure energy which is dictated by the beam size, laser power, and writing speed. A schematic of the two-photon LDW system is shown in Figure 5a. The SEM images of different BFP patterns fabricated by this LDW system at a submicron resolution are shown in Figure 5b–g. The microstructures printed by two-photon LDW with a submicron resolution could potentially be further developed for biological studies, which require micro-/nanoscale features or physical cues.

**3.5. Microscale Continuous Optical Projection Printing with BPA-Free Polycarbonates.** Although the two-photon LDW system can provide microstructures with a high resolution, its printing speed is limited by its serial writing nature as used in conventional extrusion-based 3D printers. Also, the interfaces between the printed lines could compromise the mechanical integrity of the resulting 3D structure. To address these challenges, we have developed a

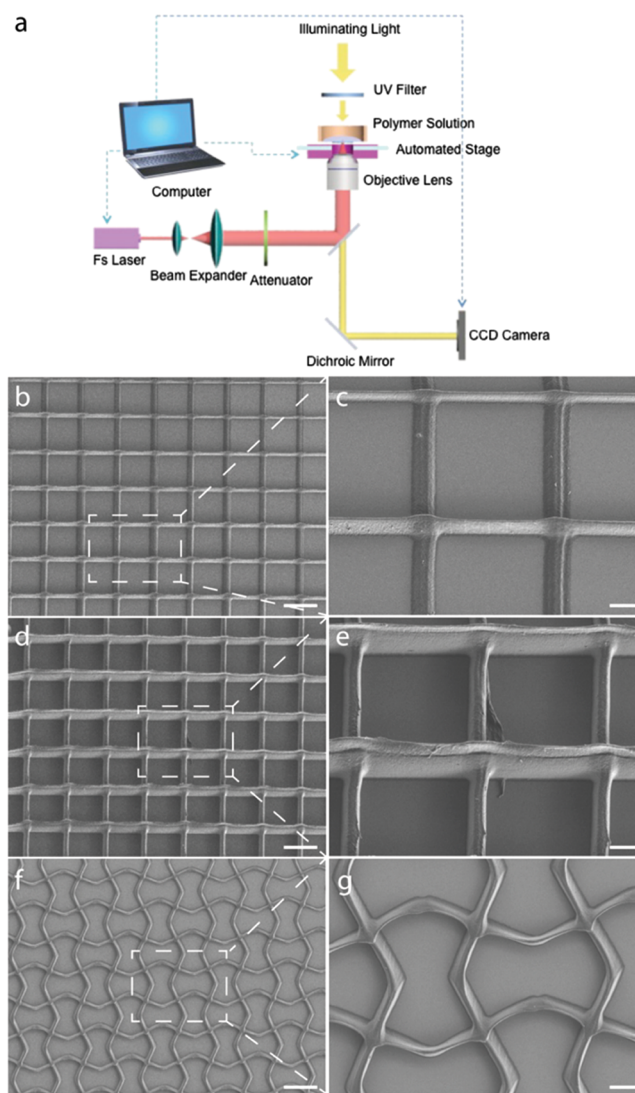


**Figure 5.** Schematic of the two-photon LDW setup (a) and SEM images of micro-/nanoscale BFP structures fabricated by the two-photon LDW (b–g). Scale bars: (b,d,f) 10 and (c,e,g) 2  $\mu$ m.

$\mu$ COP 3D printing system.<sup>26,27</sup> The  $\mu$ COP system mainly consists of a DMD, a light source, projection optics, and a motorized 3D stage (Figure 6a). All of these components are controlled by a computer to enable continuous printing of 3D objects. Instead of printing dot-by-dot or line-by-line, the  $\mu$ COP system continuously projects digital mask slices derived from the 3D design models to the prepolymer solution. By

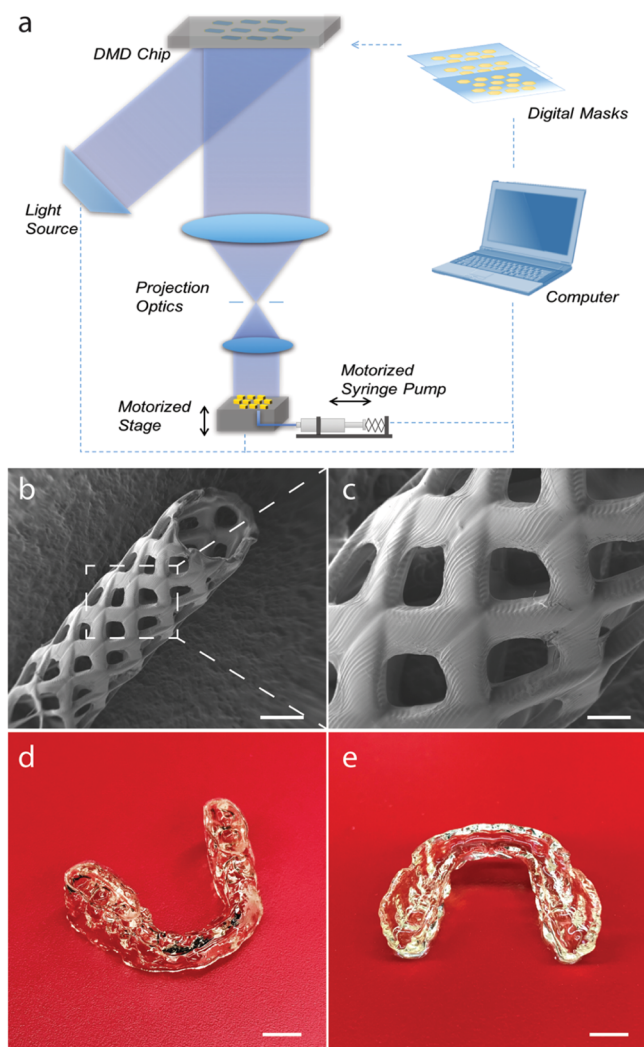


**Figure 6.** Three-dimensional printing of BFP structures with  $\mu$ COP. (a) Schematic of the  $\mu$ COP setup. (b,c) SEM images of the 3D mesh tube with BFP-4 printed by  $\mu$ COP. (d,e) Full-size mouth guard printed with BFP-1 by  $\mu$ COP. Scale bars: (b) 500  $\mu$ m, (c) 200  $\mu$ m, and (d,e) 1 cm.

simultaneously moving the motorized stage, layerless printing is achieved at a much faster speed than conventional extrusion-based 3D printers. This printing platform can create complex polymer scaffolds for both *in vitro* and *in vivo* applications, such as early-stage drug screening and tissue regeneration.<sup>35–38</sup> Our previous work has demonstrated the speed, precision, and versatility of the fabrication processes with other biomaterials such as poly(ethylene glycol) diacrylate, hyaluronic acid glycidyl methacrylate, and gelatin methacrylate.<sup>39–42</sup> However, these hydrogel materials do not have high durability, machinability, and mechanical stiffness as polycarbonate materials, which can be very desirable for some applications such as microfluidics, organ-on-a-chip, flexible biosensors, and biocompatible actuators.

To demonstrate the printability of the BFPs, we loaded the intermediate polycarbonate prepolymer solution to the  $\mu$ COP system and printed a mesh tube (Figure 6b,c). Because of the continuous layerless printing, the 3D printing of the mesh tube was completed in less than 5 min. Furthermore, we explored the potential use of these BFPs for personalized oral appliances and dental models. As a proof of concept, a full-size mouth

guard printed by the  $\mu$ COP system is shown in Figure 6d,e. Current practices to produce customized dental products usually involve molding by dental professionals and sending the molds out to the manufacturer to make the actual mouth piece, which often takes multiple visits to the dental office for fitting and optimization. Our  $\mu$ COP system combined with a library of mechanically tunable BFPs could potentially provide a desktop 3D printing platform for dentists to rapidly print personalized oral appliances and dental models on demand and significantly reduce patient visit time as well as costs.

### 3.6. Biocompatibility of the BPA-Free Polycarbonates.

To investigate the potential use of BFPs for biomedical devices, we performed a cell viability assay on four BFP formulations. More specifically, C3H10T1/2 cells, which are a commonly used adherent murine embryo fibroblast cell line, were chosen for all subsequent *in vitro* culturing studies. LIVE/DEAD staining of the BFP samples seeded with C3H10T1/2 cells demonstrated over 95% cell viability at 24, 48, and 96 h time points (Figure 7). Furthermore, a typical C3H10T1/2 fibroblast morphology was observed with cell confluence reached on all BFP formulations by 96 h (Figure 7a). These results show the biocompatibility of the BFPs to support cell growth and proliferation, highlighting the potential use of our newly developed BFPs in biomedical research and healthcare industry. For specific biomedical applications, future work will be needed to systematically evaluate the toxicity and biocompatibility of the BFPs. Furthermore, biodegradability is another important material property for biomedical devices and implants. Both *in vitro* and *in vivo* degradation tests will be needed in the future medical applications of the new BFPs because the degradation behavior of a material is closely related to its surrounding environment (e.g., the cell and enzyme activities in the lesion site of the host animal for *in vivo* implantations).

## 4. CONCLUSIONS

Polycarbonates are commonly used in medical devices and consumer products owing to their durability, high impact resistance, optical transparency, and excellent plasticity. However, they have met with a public controversy because of the presence of BPA, which is a compound used in polycarbonate production that has recently been linked to serious health risks. The vast majority of the population in the industrialized countries are exposed to BPA-containing products,<sup>12,18</sup> and a growing number of *in vivo* studies have found that BPA exposure is correlated with various health problems, such as altered behavior and disrupted neurodevelopment in children and cardiovascular diseases and diabetes in adults.<sup>12–15,43</sup> With the prevalence of BPA-containing commercial polycarbonate products, increasing societal concerns point to the demand for developing BFPs for medical devices and consumer products.

In this work, we reported, for the first time, a novel method to develop a new class of photopolymerizable BFPs that can be used in optical 3D printing to fabricate structures on both the microscale and the nanoscale. A green and robust pathway to prepare these new polycarbonates was also presented as a two-step reaction involving mild thermal ROP and low-intensity visible light-induced polymerization. The mechanical properties of these BFPs can be tuned by adjusting the ratio of the two carbonate compositions, which offers great flexibility to tailor materials for specific applications. The thermal and optical properties of these BFPs were also evaluated for potential

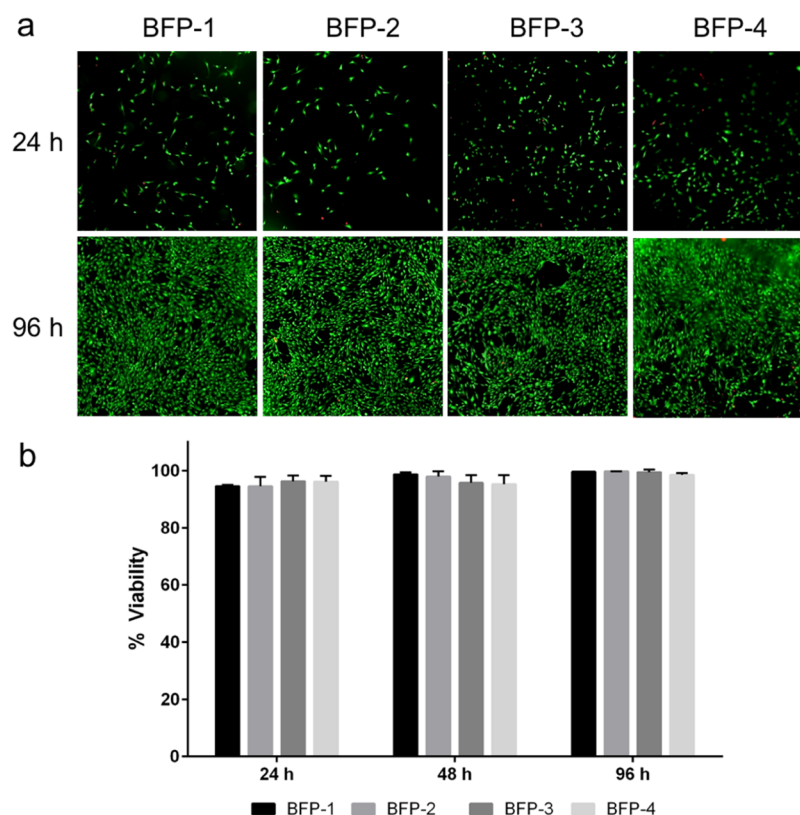


**Figure 7.** Cytotoxicity test of the BFPs with C3H10T1/2 cells. (a) LIVE/DEAD staining of C3H10T1/2 cells seeded on the four BFP formulations after 24 and 96 h. (b) Quantitative viability results of C3H10T1/2 cells grown on the four BFP formulations showing over 95% viability at 24, 48, and 96 h.

applications in the biomedical research field and the healthcare industry. Furthermore, we used two types of 3D optical printing systems—two-photon LDW and  $\mu$ COP—to demonstrate the printability of our BFPs to create both micro- and macrostructures with a great speed, flexibility, and versatility. Notably, the growth of a common fibroblast cell line (C3H10T1/2) on the BFPs also demonstrated high cell viability with the maintenance of a typical fibroblast morphology and proliferation rate, which further validated BFPs as a potential material for making biomedical devices in cell studies. Given the biocompatibility, controllable mechanical properties, and printability on the advanced optical 3D printing systems, our BFP materials would have significant impact in numerous applications including biomedical devices, tissue/organ-on-chip, biosensors, biorobotics, and healthcare products.

## ■ ASSOCIATED CONTENT

### 📄 Supporting Information

The Supporting Information is available free of charge on the ACS Publications website at DOI: 10.1021/acsami.7b18312.

TGA measurement of the polycarbonate material (BFP-1) (PDF)

## ■ AUTHOR INFORMATION

### Corresponding Authors

\*E-mail: sang-hyun.pyo@biotek.lu.se (S.-H.P.).

\*E-mail: chen168@eng.ucsd.edu (S.C.).

### ORCID

Wei Zhu: 0000-0002-2524-0866

## Author Contributions

W.Z. and S.-H.P. contributed equally to this work. W.Z., S.-H.P., and S.C. conceived the idea and designed the experiments. W.Z. and S.-H.P. led the experiments and analyzed the experimental data. S.-H.P. synthesized the materials. W.Z., S.-H.P., P.W., and J.L. performed the material characterization. W.Z., S.Y., J.A., and Y.L. performed the 3D printing. W.Z. and C.Y. designed the 3D printing structure and performed the biocompatibility study. W.Z., S.-H.P., P.W., C.Y., J.L., and S.C. wrote the manuscript.

## Funding

The work was supported by grants from the California Institute for Regenerative Medicine (RT3-07899), National Institutes of Health (R01EB021857 and R21HD090662), and National Science Foundation (CMMI-1547005 and CMMI-1644967) to S.C., and S.-H.P. was supported by the Swedish Research Council Formas for Environment, Agricultural Sciences and Spatial Planning (213-2013-1061 and 942-2016-63).

## Notes

The authors declare no competing financial interest.

## ■ ACKNOWLEDGMENTS

We thank Xuanyi Ma and Anna Koroleva-Maharajh for helpful discussions. We thank Yuan Zeng for assistance with the TGA measurement.

## ■ REFERENCES

(1) Akaraonye, E.; Keshavarz, T.; Roy, I. Production of Polyhydroxyalkanoates: The Future Green Materials of Choice. *J. Chem. Technol. Biotechnol.* **2010**, *85*, 732–743.

- (2) Chen, F.-M.; Liu, X. Advancing Biomaterials of Human Origin for Tissue Engineering. *Prog. Polym. Sci.* **2016**, *53*, 86–168.
- (3) Kucinska-Lipka, J.; Gubanska, I.; Janik, H.; Sienkiewicz, M. Fabrication of Polyurethane and Polyurethane Based Composite Fibres by the Electrospinning Technique for Soft Tissue Engineering of Cardiovascular System. *Mater. Sci. Eng., C* **2015**, *46*, 166–176.
- (4) Qazi, T. H.; Mooney, D. J.; Pumberger, M.; Geißler, S.; Duda, G. N. Biomaterials Based Strategies for Skeletal Muscle Tissue Engineering: Existing Technologies and Future Trends. *Biomaterials* **2015**, *53*, 502–521.
- (5) Chen, Q.; Liang, S.; Thouas, G. A. Elastomeric Biomaterials for Tissue Engineering. *Prog. Polym. Sci.* **2013**, *38*, 584–671.
- (6) Campoccia, D.; Montanaro, L.; Arciola, C. R. A Review of the Biomaterials Technologies for Infection-Resistant Surfaces. *Biomaterials* **2013**, *34*, 8533–8554.
- (7) Li, X.; Franke, A. A. Improvement of Bisphenol A Quantitation from Urine by LCMS. *Anal. Bioanal. Chem.* **2015**, *407*, 3869–3874.
- (8) Huygh, J.; Clotman, K.; Malarvannan, G.; Covaci, A.; Schepens, T.; Verbrugghe, W.; Dirinck, E.; Van Gaal, L.; Jorens, P. G. Considerable Exposure to the Endocrine Disrupting Chemicals Phthalates and Bisphenol-A in Intensive Care Unit (ICU) Patients. *Environ. Int.* **2015**, *81*, 64–72.
- (9) Gimeno, P.; Spinau, C.; Lassu, N.; Maggio, A.-F.; Brenier, C.; Lempereur, L. Identification and Quantification of Bisphenol A and Bisphenol B in Polyvinylchloride and Polycarbonate Medical Devices by Gas Chromatography with Mass Spectrometry. *J. Sep. Sci.* **2015**, *38*, 3727–3734.
- (10) Feng, J.; Zhuo, R.-X.; Zhang, X.-Z. Construction of Functional Aliphatic Polycarbonates for Biomedical Applications. *Prog. Polym. Sci.* **2012**, *37*, 211–236.
- (11) Fukuoka, S.; Hachiya, H.; Matsuzaki, K.; Miyaji, H. Industrial Process for Production of High-Purity Diphenyl Carbonate. U.S. Patent 7,812,189 B2, 2010.
- (12) Rochester, J. R. Bisphenol A and Human Health: A Review of the Literature. *Reprod. Toxicol.* **2013**, *42*, 132–155.
- (13) Melzer, D.; Rice, N. E.; Lewis, C.; Henley, W. E.; Galloway, T. S. Association of Urinary Bisphenol A Concentration with Heart Disease: Evidence from NHANES 2003/06. *PLoS One* **2010**, *5*, No. e8673.
- (14) Lang, I. A. Association of Urinary Bisphenol A Concentration with Medical Disorders and Laboratory Abnormalities in Adults. *JAMA, J. Am. Med. Assoc.* **2008**, *300*, 1303–1310.
- (15) Braun, J. M.; Kalkbrenner, A. E.; Calafat, A. M.; Yolton, K.; Ye, X.; Dietrich, K. N.; Lanphear, B. P. Impact of Early-Life Bisphenol A Exposure on Behavior and Executive Function in Children. *Pediatrics* **2011**, *128*, 873–882.
- (16) Chapin, R. E.; Adams, J.; Boekelheide, K.; Gray, L. E.; Hayward, S. W.; Lees, P. S. J.; McIntyre, B. S.; Portier, K. M.; Schnorr, T. M.; Selevan, S. G.; Vandenberg, J. G.; Woskie, S. R. NTP-CERHR Expert Panel Report on the Reproductive and Developmental Toxicity of Bisphenol A. *Birth Defects Res., Part B* **2008**, *83*, 157–395.
- (17) Calafat, A. M.; Ye, X.; Wong, L.-Y.; Reidy, J. A.; Needham, L. L. Exposure of the U.S. Population to Bisphenol A and 4-Tertiary-Octylphenol: 2003–2004. *Environ. Health Perspect.* **2008**, *116*, 39–44.
- (18) Calafat, A. M.; Kuklenyik, Z.; Reidy, J. A.; Caudill, S. P.; Ekong, J.; Needham, L. L. Urinary Concentrations of Bisphenol A and 4-Nonylphenol in a Human Reference Population. *Environ. Health Perspect.* **2005**, *113*, 391–395.
- (19) Huang, H.; Li, Y.; Liu, J.; Tong, J.; Su, X. Detection of Bisphenol A in Food Packaging Based on Fluorescent Conjugated Polymer PPES03 and Enzyme System. *Food Chem.* **2015**, *185*, 233–238.
- (20) Pyo, S.-H.; Persson, P.; Mollaahmad, M. A.; Sørensen, K.; Lundmark, S.; Hatti-Kaul, R. Cyclic Carbonates as Monomers for Phosgene- and Isocyanate-Free Polyurethanes and Polycarbonates. *Pure Appl. Chem.* **2011**, *84*, 637–661.
- (21) Pyo, S.-H.; Hatti-Kaul, R. Selective, Green Synthesis of Six-Membered Cyclic Carbonates by Lipase-Catalyzed Chemospecific Transesterification of Diols with Dimethyl Carbonate. *Adv. Synth. Catal.* **2012**, *354*, 797–802.
- (22) Pyo, S.-H.; Persson, P.; Lundmark, S.; Hatti-Kaul, R. Solvent-Free Lipase-Mediated Synthesis of Six-Membered Cyclic Carbonates from Trimethylolpropane and Dialkyl Carbonates. *Green Chem.* **2011**, *13*, 976–982.
- (23) Pyo, S.-H.; Hatti-Kaul, R. Chlorine-Free Synthesis of Organic Alkyl Carbonates and Five- and Six-Membered Cyclic Carbonates. *Adv. Synth. Catal.* **2016**, *358*, 834–839.
- (24) Zhang, W.; Chen, S. Femtosecond Laser Nanofabrication of Hydrogel Biomaterial. *MRS Bull.* **2011**, *36*, 1028–1033.
- (25) Zhang, W.; Han, L.-H.; Chen, S. Integrated Two-Photon Polymerization with Nanoimprinting for Direct Digital Nanomanufacturing. *J. Manuf. Sci. Eng.* **2010**, *132*, 030907.
- (26) Zhang, A. P.; Qu, X.; Soman, P.; Hribar, K. C.; Lee, J. W.; Chen, S.; He, S. Rapid Fabrication of Complex 3D Extracellular Microenvironments by Dynamic Optical Projection Stereolithography. *Adv. Mater.* **2012**, *24*, 4266–4270.
- (27) Zhu, W.; Li, J.; Leong, Y. J.; Rozen, I.; Qu, X.; Dong, R.; Wu, Z.; Gao, W.; Chung, P. H.; Wang, J.; Chen, S. 3D-Printed Artificial Microfish. *Adv. Mater.* **2015**, *27*, 4411–4417.
- (28) Helou, M.; Miserque, O.; Brusson, J.-M.; Carpentier, J.-F.; Guillaume, S. M. Organocatalysts for the Controlled “immortal” ring-opening Polymerization of Six-Membered-Ring Cyclic Carbonates: A Metal-Free, Green Process. *Chem.—Eur. J.* **2010**, *16*, 13805–13813.
- (29) Engler, A. J.; Sen, S.; Sweeney, H. L.; Discher, D. E. Matrix Elasticity Directs Stem Cell Lineage Specification. *Cell* **2006**, *126*, 677–689.
- (30) Hribar, K. C.; Choi, Y. S.; Ondeck, M.; Engler, A. J.; Chen, S. Digital Plasmonic Patterning for Localized Tuning of Hydrogel Stiffness. *Adv. Funct. Mater.* **2014**, *24*, 4922–4926.
- (31) Choi, Y. S.; Vincent, L. G.; Lee, A. R.; Kretschmer, K. C.; Chirasatitsin, S.; Dobke, M. K.; Engler, A. J. The Alignment and Fusion Assembly of Adipose-Derived Stem Cells on Mechanically Patterned Matrices. *Biomaterials* **2012**, *33*, 6943–6951.
- (32) Vincent, L. G.; Choi, Y. S.; Alonso-Latorre, B.; del Álamo, J. C.; Engler, A. J. Mesenchymal Stem Cell Durotaxis Depends on Substrate Stiffness Gradient Strength. *Biotechnol. J.* **2013**, *8*, 472–484.
- (33) Isenberg, B. C.; DiMilla, P. A.; Walker, M.; Kim, S.; Wong, J. Y. Vascular Smooth Muscle Cell Durotaxis Depends on Substrate Stiffness Gradient Strength. *Biophys. J.* **2009**, *97*, 1313–1322.
- (34) Mehr, M. Y.; van Driel, W. D.; Jansen, K. M. B.; Deeben, P.; Boutelje, M.; Zhang, G. Q. Photodegradation of Bisphenol A Polycarbonate under Blue Light Radiation and Its Effect on Optical Properties. *Opt. Mater.* **2013**, *35*, 504–508.
- (35) Zhu, W.; Ma, X.; Gou, M.; Mei, D.; Zhang, K.; Chen, S. 3D Printing of Functional Biomaterials for Tissue Engineering. *Curr. Opin. Biotechnol.* **2016**, *40*, 103–112.
- (36) Hribar, K. C.; Soman, P.; Warner, J.; Chung, P.; Chen, S. Light-Assisted Direct-Write of 3D Functional Biomaterials. *Lab Chip* **2014**, *14*, 268–275.
- (37) Ma, X.; Qu, X.; Zhu, W.; Li, Y.-S.; Yuan, S.; Zhang, H.; Liu, J.; Wang, P.; Lai, C. S. E.; Zanella, F.; Feng, G.-S.; Sheikh, F.; Chien, S.; Chen, S. Deterministically Patterned Biomimetic Human iPSC-Derived Hepatic Model via Rapid 3D Bioprinting. *Proc. Natl. Acad. Sci. U.S.A.* **2016**, *113*, 2206–2211.
- (38) Zhu, W.; Qu, X.; Zhu, J.; Ma, X.; Patel, S.; Liu, J.; Wang, P.; Lai, C. S. E.; Gou, M.; Xu, Y.; Zhang, K.; Chen, S. Direct 3D Bioprinting of Prevascularized Tissue Constructs with Complex Microarchitecture. *Biomaterials* **2017**, *124*, 106–115.
- (39) Qu, X.; Zhu, W.; Huang, S.; Li, Y.-S.; Chien, S.; Zhang, K.; Chen, S. Relative Impact of Uniaxial Alignment vs. Form-Induced Stress on Differentiation of Human Adipose Derived Stem Cells. *Biomaterials* **2013**, *34*, 9812–9818.
- (40) Soman, P.; Chung, P. H.; Zhang, A. P.; Chen, S. Digital Microfabrication of User-Defined 3D Microstructures in Cell-Laden Hydrogels. *Biotechnol. Bioeng.* **2013**, *110*, 3038–3047.
- (41) Suri, S.; Han, L.-H.; Zhang, W.; Singh, A.; Chen, S.; Schmidt, C. E. Solid Freeform Fabrication of Designer Scaffolds of Hyaluronic Acid for Nerve Tissue Engineering. *Biomed. Microdevices* **2011**, *13*, 983–993.

(42) Cha, C.; Soman, P.; Zhu, W.; Nikkhah, M.; Camci-Unal, G.; Chen, S.; Khademhosseini, A. Structural Reinforcement of Cell-Laden Hydrogels with Microfabricated Three Dimensional Scaffolds. *Biomater. Sci.* **2014**, *2*, 703–709.

(43) Vandenberg, L. N.; Maffini, M. V.; Sonnenschein, C.; Rubin, B. S.; Soto, A. M. Bisphenol-A and the Great Divide: A Review of Controversies in the Field of Endocrine Disruption. *Endocr. Rev.* **2009**, *30*, 75–95.